The Polstar UV Spectropolarimetry Mission

Richard IGNACE[1,*] and Paul SCOWEN[2]

[1] East Tennessee State University, Johnson City, TN 37615, USA
[2] Code 667, Exoplanets & Stellar Astrophysics Lab, NASA/GSFC, USA
[*] Corresponding author: ignace@etsu.edu

Abstract

The *Polstar* small explorer concept is for an ultraviolet (UV) spectropolarimetry space telescope mission with a focus on massive star astrophysics. The instrument waveband will be from 115 nm – 286 nm for spectroscopy and 122 nm – 286 nm for polarimetry. All 4 Stokes parameters, IQUV, will be measured at a resolving power of $R = 20,000$ (15 km/s velocity resolution). The telescope aperture will be 40 cm with an effective area of about 22 cm^2 at a reference wavelength of 150 nm. The thrust of the science goals will be to determine the astrophysics of angular momentum exchange and transport, and consequences for massive star properties and evolution. This includes the effects of rapid to critical rotation for individual stars (magnetic and non-magnetic), and the effects of mass transfer for massive binaries, including identification of stripped core stars. If selected by the NASA/SMEX program, *Polstar* would launch around 2031 and observe ~ 300 stars to achieve science goals. The mission will include a Guest Observer program to advance discovery in other areas of astrophysics.

1. Introduction

Massive stars are hot, UV-bright, luminous stars with short lifetimes that terminate in dramatic style leaving behind compact object remnants (Langer, 2012). Moreover, they are central in the cosmic narrative for so many other areas of astrophysics. Massive stars are important for galaxy evolution as sites for nucleosynthesis and spewing metals throughout galaxies, making Earth-like worlds possible (Nomoto et al., 2013). The story of massive stars further intersects with gravitational wave detections involving stellar mass black holes (e.g., Belczynski et al., 2010).

However, a full story of massive stars themselves continues to be a topic of debate and investigation (e.g., Vink, 2022). We understand now that massive stars are born into binaries, triples, or higher multiples (Sana et al., 2012; Kummer et al., 2023). Relative to the critical speed of breakup at the stellar equator, nearly all are rapidly rotating (above $\sim$30%), and some are rotating near critical (above 90%). Those that are slowly rotating are likely magnetic (Ud-Doula et al., 2009). Binarity combined with the incidence of runaway stars (Renzo et al., 2019) and high rotation rates (Penny, 1996; Huang et al., 2010) makes clear that massive stars can

undergo substantive interactions, such as mass transfer, common envelope, and even mergers (e.g., Nathaniel et al., 2024). All of these involve the exchange of angular momentum, including orbital evolution and stellar spin up (Podsiadlowski et al., 1992; Toonen et al., 2020). It remains unclear how much spin-up occurs, how angular momentum is transported throughout stellar interiors, and how much is conserved or lost to the system during mass exchange.

Although stellar evolution is driven by gravity and therefore by mass, issues of rotation are consequential. The *Polstar* mission will bring ultraviolet (UV) spectropolarimetry to bear on outstanding questions concerning angular momentum exchange and internal transport – UV because this where massive stars have peak brightnesses, spectroscopy because of the strong resonance lines and wide range of ion species to be found in the UV, and polarimetry because it probes geometry (e.g., Clarke, 2010). The latter is the novel aspect of *Polstar*. The stars are unresolved, and the issues of fast rotation, binarity, and magnetism are intrinsically aspherical in nature. Polarization is sensitive to deviations from sphericity and will provide new diagnostics for advancing our understanding of massive stars. This contribution provides an overview of UV spectral and polarimetric diagnostics and a summary of the *Polstar* design and capabilities.

2. Spectropolarimetric Diagnostics for Massive Stars

Polarization is measured using Stokes Parameters I, Q, U, and V. Stokes-I refers to the total measure of light. Stokes-V is a measure of circular polarization. Two parameters are needed for linear polarization, Q and U. It is typical to measure polarization in relative terms. For Stokes fluxes F_I, F_Q, and F_U, relative parameters are $q = F_Q/F_I$, and $u = F_U/F_I$. Then the degree of polarization p and polarization position angle $\psi_{\rm p}$ become

$$p = \sqrt{q^2 + u^2}, \text{ and } \tan 2\psi_{\rm p} = u/q.$$

For applications to massive stars at UV and visible wavelengths, polarizations are typically small, with 1% polarization being fairly sizable. It is often (but not always) convenient to treat linear and circular polarizations separately, with circular polarization $p_V = F_V/F_I$.

2.1. Continuum Polarization

2.1.1. Polar Brightening and Gravity Darkening

Critical rotation is typically defined as $v_{\rm crit} = \sqrt{GM/R}$, for stellar mass M, stellar radius R, and gravitational constant G. When the equator of a star rotates at this critical speed, gas is no longer bound. However, other effects also come into play. For example, at high rotations the star is distorted from spherical ("oblateness"), making radius a function of latitude. Additionally, the surface temperature becomes a function of latitude, being hotter toward the pole ("polar brightening") and lower at the equator ("gravity darkening"), relative to a non-rotating star (von Zeipel, 1924; Espinosa Lara and Rieutord, 2011, (ELR)). As gravity drops at the equator, a star can become closer to the Eddington limit. Consequently, gravity can be reduced at the equator by rotation and radiation both (Maeder and Meynet, 2000).

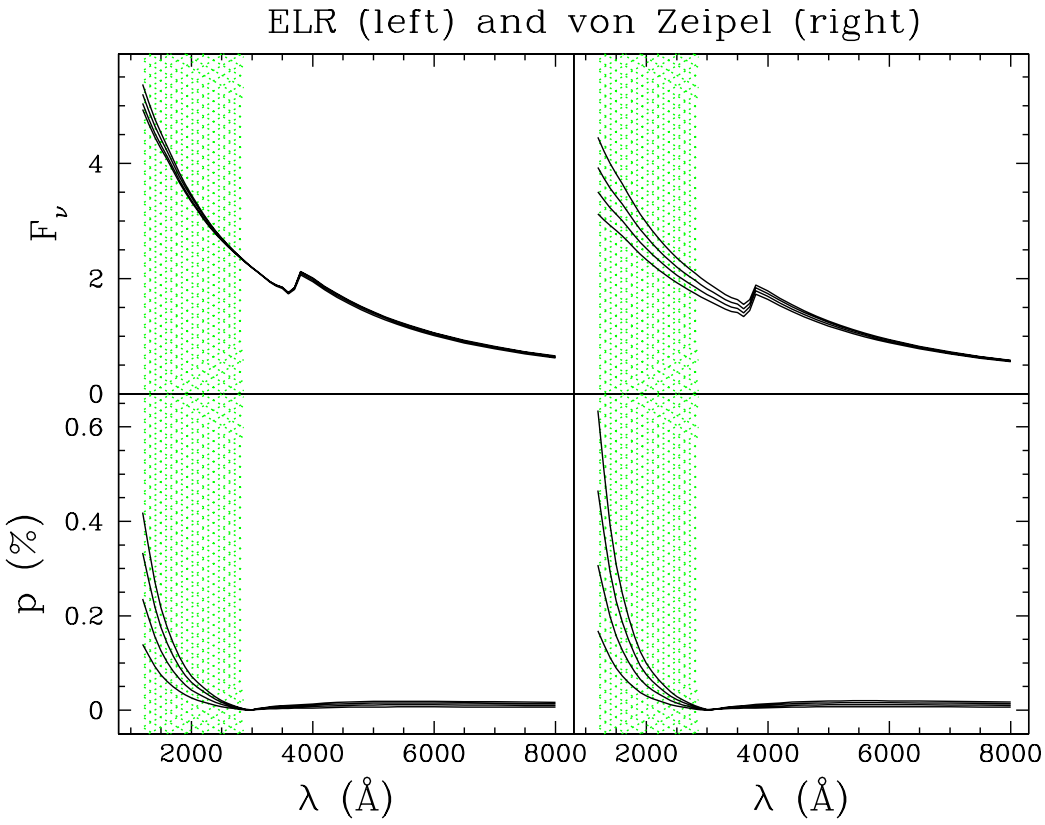

Figure 1: Net polarization produced from a gravity darkened B1V star ($T_{\rm eff} = 25,700$ K when not rotating) at $\omega = 0.80$ (lowest polarization), 0.90, 0.95, and 0.975 (highest polarization) for the star viewed edge-on. Top is the flux distribution; bottom is polarization. Left is for ELR; right is for von Zeipel. Green shading is the *Polstar* waveband.

Let ω be a dimensionless parameter for rotation relative to critical (now defined to account for oblateness and radiation as well), with $\omega < 1$ for gas at the equator to remain bound. The effects of near-critical rotation tend to scale as $\sqrt{1-\omega^2}$, meaning that even up to 50% of critical, geometrical distortions are only at the level of 10%. It is rotation rates above about 80% where rotational influences can become dominant. One consequence for *Polstar* is a net polarization from the stellar atmosphere (Harrington and Collins, 1968; Collins et al., 1991). Towards the FUV, the strongly aspherical star and temperature distribution can lead to significant net polarizations of around 1% and more (see Fig. 1 for the conservative case of a B1V star). Ground-based efforts have made sensitive detections of this effect in a limited number of bright stars at much lower levels in the optical band. Gravity darkening makes specific predictions for polarization with a dramatic rise toward the FUV. Measurements of that distribution is one of the few ways to ascertain precisely how close to critical the fastest rotating stars get.

2.1.2. Circumstellar Scattering

For hot massive stars, H is highly ionized (and for Wolf-Rayet [WR] stars, He is ionized). The dominant polarigenic continuum opacity is electron scattering. The optical depth through a circumstellar medium is of the form

$$\tau_{\rm e} = \int n_{\rm e}\, \sigma_T\, dr, \tag{1}$$

where $\tau_{\rm e}$ is the electron optical depth along a radial integration of the electron density $n_{\rm e}$, and σ_T is the Thomson scattering cross-section. The latter is fairly low at $\sigma_T = 6.656 \times 10^{-25}$ cm^2. The electron optical depth is thus column depth multiplied by the cross-section. The column depth is approximately a product of the base density of the medium (e.g., the wind base or the inner edge of a disk) multiplied by a characteristic length scale (generally the stellar radius). For a spherical wind, the base density scales roughly as $n_0 \sim \dot{M}/4\pi\,\mu_{\rm e}\, m_H\, R^2\, v_\infty$, for R the radius, m_H the mass of H, v_∞ the wind terminal speed, and $\mu_{\rm e}$ the mean molecular weight per free electron. For O and B stars, the latter will be of order unity; for WRs, it may be around 2 or 3. The expression does not account for integrating through the wind acceleration zone, which may increase the density scale by a factor of a few. Rough estimates for electron optical depths of *Polstar* target categories range from negligible for B winds to a few for WR winds. However, the disks of Be stars and of interacting binaries can have optical depths of order unity or more.

2.2. Line Polarization Effects

2.2.1. Öhman Effect

The Öhman effect refers to a polarization change across rotationally broadened photospheric lines (Öhman, 1946; Bailey et al., 2024b). The isovelocity zones of a rotating star are vertical strips, ranging from $-v\sin i$ to $+v\sin i$. For an $x-y$ sky coordinate system, with y the projection of the star's rotation axis, the strips are parallel to y. A velocity bin of Δv maps to a strip of width Δx. This is approximate since thermal/turbulent broadening causes strips not to have geometrically sharp edges.

To illustrate, ignore rotational distortion and assume the star is spherical. It will have a centro-symmetric pattern of limb polarization, which is also wavelength-dependent (generally larger toward UV wavelengths). Thus rotational broadening creates a breaking of symmetry, since a strip at x, corresponding to a line-of-sight velocity shift $v_{\rm z}$, is relatively more absorbing of polarized light (assuming a pure absorption line). The result is that the remainder of the centro-symmetric pattern no longer cancels.

The Stokes-Q polarization shows a triple peak pattern, with two negative polarizations for the line wings, and a positive one at line center. By contrast the Stokes-U polarization is antisymmetric and zero at line center. The polarization tends to be weaker, and weaker in U than Q. The detailed profile shapes are sensitive to the limb polarization profile, from center to limb, so can be used to probe stellar atmosphere models.

2.2.2. Zeeman Effect

The Zeeman effect is well known for producing line splitting of spectral lines in the presence of magnetism. However in astrophysical contexts, observed splittings are rare, normally requiring strong fields ($\sim$MG). More typical are weaker fields leading to linear and circular

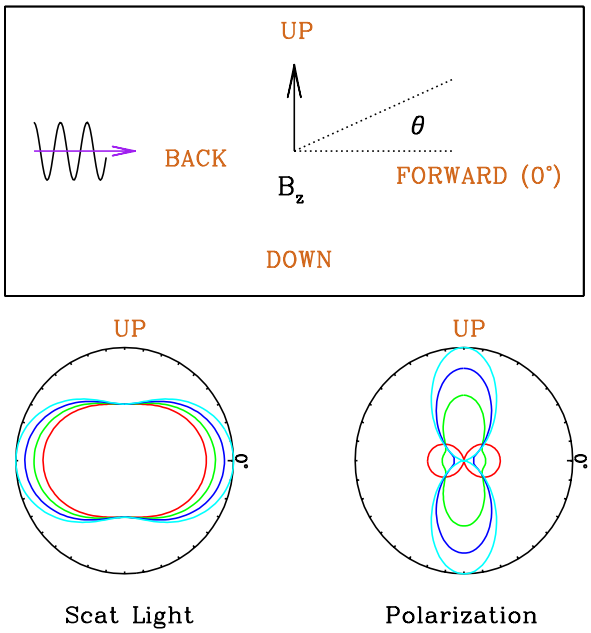

Figure 2: Top: Simple scattering geometry to illustrate the Hanle effect. Unpolarized radiation is incident from the left on a scatterer where there is a vertical magnetic field (B_z). Light is scattered by angle θ, with 0° being forward, and other directions as labeled. Bottom: Scaled redistribution of scattered light and polarization by the Hanle effect for 5 field strengths, from $B_z = 0$ for magenta to the "saturated" limit for large B_z (red), shown in the form of polar plots. Based on expressions (26)–(28) from Ignace et al. (1999).

polarizations. These arise the transverse and longitudinal Zeeman effects, respectively (e.g., Stenflo, 1994). For modest field strengths (∼kG), the lines are not distinctly split (although Zeeman broadening may be detected); instead, polarization results from considerations of spectral line gradients. The transverse effect produces linear polarization and derives from a second derivative of the Stokes-I profile shape and is proportional to the square of the field strength, B^2. Easier to measure is circular polarization from the longitudinal effect, which is linear in B, derives from a first derivative, and is antisymmetric about line center.

Detection of the Zeeman effect in massive stars is challenging. Line broadening tends to lessen the first derivative, so that polarization scales as $v_Z/v_{\rm broad}$. Here $v_Z = c\Delta\lambda_Z/\lambda_0$ for the Zeeman effect in velocity units, with $\Delta\lambda_Z$ the Zeeman shift for a line at λ_0. Then $v_{\rm broad}$ may be thermal, rotational, or wind broadening. This challenge has been successfully overcome for measuring surface stellar magnetism through a co-adding procedure known as "LSD" to combine numerous spectral lines and increase signal-to-noise as $\sqrt{N}$, for N the number of lines (e.g., Donati and Landstreet, 2009). One advantage of UV spectropolarimetry is it offers far more lines as compared to the optical in order to measure magnetism in O stars, in particular numerous iron lines (Folsom et al., 2022).

2.2.3. *Hanle Effect*

This is another diagnostic of magnetism from spectral line formation. It refers to an especially weak field limit in which the Zeeman broadening has not fully lifted the degeneracy of the magnetic sublevels, when the Zeeman splitting is of order the natural line broadening. In laboratory atomic physics, one controls the field and infers level lifetimes (i.e., the inverse of Einstein A-values). In astrophysics, the situation is reversed.

The Hanle effect operates in resonance scattering lines and leads to linear polarization effects. In classical terms the harmonic oscillator of the radiating dipole is caused to precess at the Larmor frequency, ω_L. Consequently, magnetic sensitivity is achieved on the order of $\omega_L \sim A$, which tends to be 0.1–100 G fields, depending on the A-value, but typically largerfield strengths for lines of shorter wavelength since $A \sim 1/\lambda^3$.

The Hanle effect has not been observed in massive stars, although it has been successfully employed in solar studies (e.g., Stenflo, 2013). The Hanle effect amounts to redistribution of scattered light (see Fig. 2). UV is critical for massive star applications since that is where scattering resonance lines are found. There are three main points for use of the Hanle effect (Ignace et al., 1997). (1) The effect operates in lines whether photospheric or circumstellar. If circumstellar, the Hanle effect allows to probe directly the magnetic field strength and topology at levels that are difficult for the Zeeman effect. (2) Resonance lines have vastly higher cross-sections than electron scattering. For targets with low optical depth circumstellar media in electron scattering, resonance line polarization may still be significant. (3) A multiline approach is key for extracting information about the magnetism. For example, not all lines are Hanle sensitive. Common UV resonance lines for massive stars are Li-like doublets for which one component produces no resonance polarization, nor Hanle effect. That component serves as a control to infer magnetic detection using the Hanle sensitive one.

2.2.4. *Dilution Effect*

Winds and disks of massive stars show spectral lines that tend to be resonance or recombination. These lines can form over vastly different volumes of the circumstellar environment, subject to ionization distribution and detailed NLTE level populations. In some cases a particular spectral transition may form in a region where line photons are not much scattered by the electrons. Traditionally, polarization is measured as a ratio of polarized flux to total flux. When the line photons are not scattered, they contribute to the total flux and reduce the polarization owing to higher normalization relative to the neighboring continuum (see examples in Fig. 3). This is the "dilution effect", because the polarization flux will not have changed yet the total flux has (e.g., Harries et al., 1998).

The dilution effect is useful for two reasons: first it demonstrates the presence of intrinsic source polarization, because the interstellar polarization is not subject to dilution. Second, the dilution may be so severe as to yield a measure of the interstellar polarization at that wavelength. There is in general no reason for the continuum and interstellar polarizations to have the same position angle (PA), so severe dilution of polarization may be attended by an observed rotation

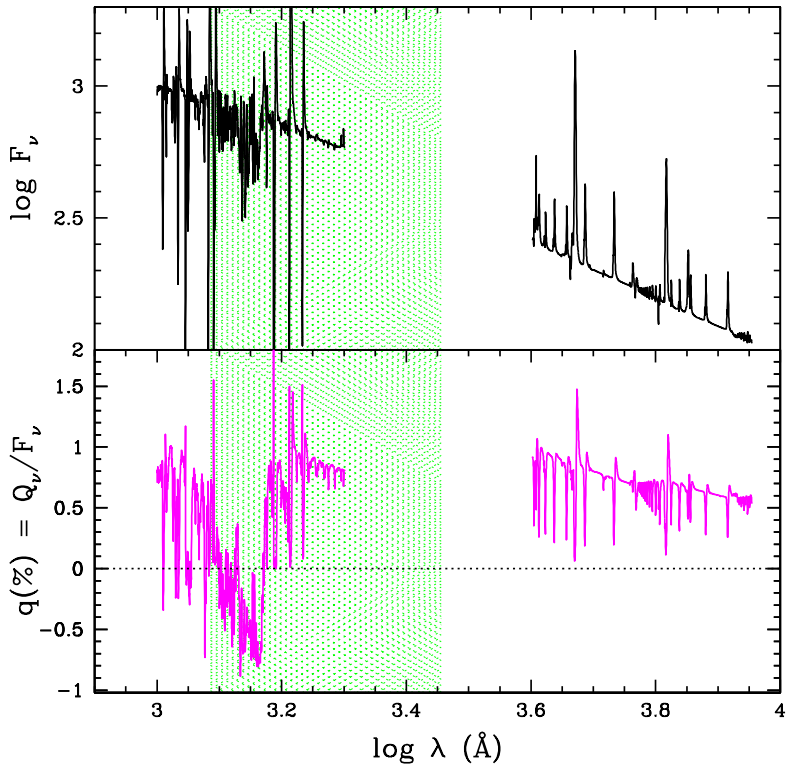

Figure 3: Synthetic spectropolarimetry for a WR star using CMFGEN (Hillier, 1994). The wind is axisymmetric with an equatorial density of 3.3× great than the pole. Top is a relative flux; bottom is the linear polarization q, where Q_ν is the polarized flux. Note the dilution effect in numerous lines for both UV and optical. The change in sign for the UV arises from iron-line blanketing and signifies a 90° position angle (PA) change. Green shading is the *Polstar* waveband.

in PA across the emission line due to the interstellar contribution.

2.2.5. Line Absorption Effect

Complex circumstellar structures can lead to differential absorption effects by line opacity in relation to where scattering polarization in the continuum is formed. There are two main opportunities of interest. First is line blanketing. In a study of the interacting binary β Lyr combining UV continuum polarization from WUPPE with ground-based optical polarization from HPOL, the polarization is seen to rotate by 90 degrees (Hoffman et al., 1998). A PA rotation is a clear signature for a change in geometry. For β Lyr the PA rotation began shortward of the Balmer jump and persisted into the UV. The former is indicative of higher absorbing bound-free opacity in the accretion disk of the system; the continuation into the UV from a forest of absorbing iron lines . However, the polarization was not eliminated, only rotated, and suggested a bipolar jet outflow from the disk, consistent with with evidence from optical interferometry (Harmanec et al., 1996). A different example of blanketing is seen in Figure 3, now for an axisymmetric WR wind with 3.3× higher density at the equator than the pole. The sign change in polarization at UV wavelengths arises from iron line blanketing, with net

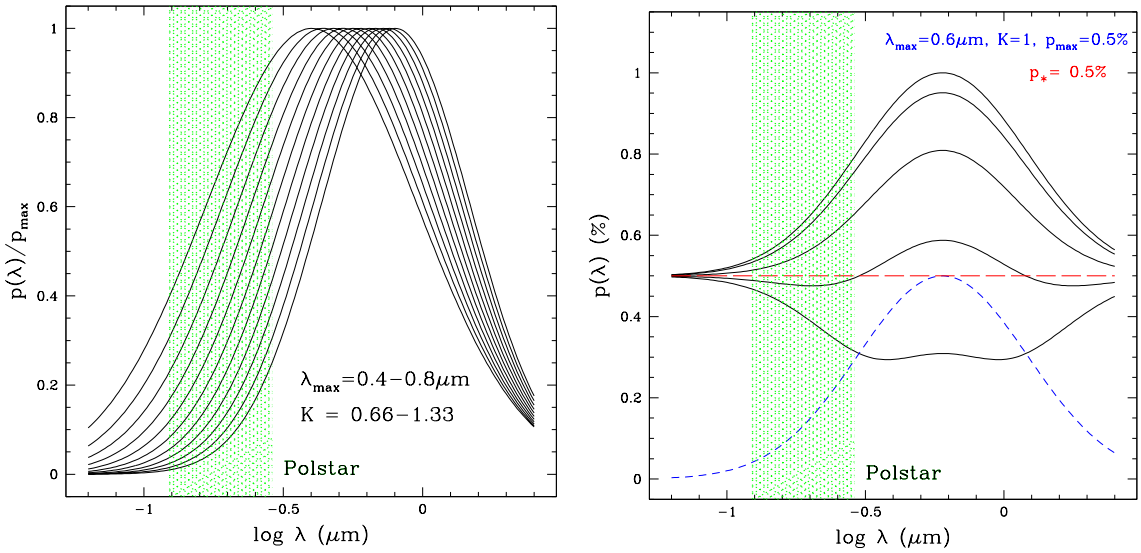

Figure 4: Left: Several Serkowski Law curves plotted for a range of $\lambda_{\max}$ and K values as indicated. The polarization is normalized to $p_{\max}$. The green hatch is the *Polstar* waveband, where interstellar polarization is rapidly dropping. Right: Illustration for how Thomson scattering and interstellar polarization could combine. Blue is the Serkowski Law; red is the stellar polarization. Black curves are combinations in which the PA between the two differ from 0° to 90° in 18° increments.

polarization coming from scattering by the less opaque polar wind.

Our second example pertains to differential absorption from complex structures in a cyclic fashion. The WR star WR 6 shows variation in polarization across the strong HeII 4686 emission line. The variation is peculiar in that polarization is reduced over redshifted velocities showing a linear feature in a $q-u$ diagram, whereas a loop is traced for blueshifted velocities (a "blue loop"). The polarization for the redshifted portion of the line follows the standard dilution effect. The blue loops signify something else.

WR 6 is a candidate for a co-rotating interaction region (CIR; St-Louis et al., 2018). A CIR is a spiral structure threading a wind owing to the presence of a brightness enhancement at the stellar surface. The enhancement drives a faster wind leading to a shock and post-shock cooling region, which in the co-rotating frame takes on the shape of a spiral. For an outflowing wind, Ignace et al. (2023) demonstrated that such a structure could indeed account for the blue loop, for those rotational phases when the CIR is passing in front of the stellar photosphere with limb polarization. *Polstar* will provide access to a rich spectrum of UV lines combining velocity shift information with polarimetry as demonstrated for WR 6.

2.3. Interstellar Polarization

As starlight passes through the interstellar medium, it obtains a linear polarization even if the star is spherical This arises from interstellar magnetism aligning dust grains, which then absorb a preferential sense of polarized light, thereby acting as an absorptive filter leaving a residual polarization orthogonal to the direction of grain alignment. The interstellar medium

Table 1: *Polstar* Attributes

Aperture	40 cm
$A_{\rm eff}$ @150 nm	22 cm^2
Waveband (Spec)	115–286 nm
Waveband (Pol)	122–286 nm
Resolving Power	20,000[a]

[a] Corresponds to 15 km/s velocity resolution.

Table 2: Instrument Characteristics

Subexposure	δt	2 s-100 s
Exposure	$t_{\rm exp}$	$6 \times \delta t$
Source Count Rate	$\dot{S}_*$	counts/s
Source Counts	S_*	$\dot{S}_* \, \delta t$
Source Noise	N_*	$\sqrt{S_*}$
Read Noise	N_R	5.4/subexposure
Dark Current	$\dot{S}_D$	0.06 Hz/pix
Dark Noise	N_D	$\sqrt{\dot{S}_D \delta t}$

thus imposes a polarization of some amplitude at fixed PA, but which is wavelength-dependent. The form of this polarization is well-modeled by the Serkowski Law (Serkowski et al., 1975), with the following form:

$$p_\lambda = p_{\rm max} \, e^{-K \ln^2(\lambda_{\rm max}/\lambda)}, \tag{2}$$

where $p_{\rm max}$ is the maximum polarization at $\lambda = \lambda_{\rm max}$, and K controls the width of the curve. For a reasonably large sample, $K \approx 1.66 \, \lambda_{\rm max}(\mu m)$ with $\lambda_{\rm max}$ ranging from 0.4 to 0.8 μm (e.g., Whittet et al., 1992).

Example plots of the Serkowski Law are shown in Figure 4, left side. These are for a range of $\lambda_{\rm max}$ values, with K determined by the relation above. The curves are normalized to $p_{\rm max}$. The right panel figure combines a flat stellar polarization from Thomson scattering. The different curves result from changing the PA between the star and interstellar, as explained in the caption. Observing in the UV with *Polstar* has the advantage that interstellar polarization is dropping and becoming far less confounding to stellar studies.

3. The Polstar Science Theme

The *Polstar* mission concept involves a UV spectropolarimeter as summarized in Table 1. The telescope will have a 40 cm aperture with an effective area of about 22 cm^2 at a fiducial wavelength of 150 nm (near the important CIV doublet). Spectroscopy will be available from 115 to 286 nm, providing for observations from Lyα to the MgII doublet. Polarimetric sensitivity ends at 122 nm. Spectropolarimetry will be achieved from the NV doublet to MgII, to include numerous important diagnostic lines that will be observed at $R = 20000$.

3.1. Science Objectives

The goal of the *Polstar* mission is to understand better the lives of massive stars and their impacts on galaxy evolution. The theme is closely aligned with many priorities of the current and recent Decadal Surveys and the NASA Astrophysics Roadmap. Specifically we seek to understand angular momentum evolution in massive stars. Essentially all massive stars are born into binaries (or triples, and even higher orders). Moreover, nearly all massive multiples

will exchange mass at some time, often short-lived yet crucially important phases. Indeed, mergers are expected in some cases. The interactions imply not only mass transfer (whether conservative or non-conservative) but attendant exchanges in angular momentum. Issues of angular momentum can lead to spin-up or spin-down of stars, and govern the evolution of binary orbits.

The *Polstar* team has developed three main science categories to be addressed with UV spectropolarimetry:

1. We seek to understand better the origin of rotational characteristics observed in massive stars. Several of the brightest massive stars in the sky are in fact in near-critical rotation (e.g., Achernar, ζ Pup, and ε Sgr, to name a few; Domiciano de Souza et al., 2003; Bailey et al., 2024a,b).

2. A better understanding of how rapid rotation affects the surfaces of massive stars. Here rapid need not be critical. Critical rotation leads to distortion of the isopotential of the star, accompanied by polar brightening and equatorial darkening. However, many massive stars are rotating only around 30% of critical, sufficient to induce mixing which is predicted (and observed) to enhance surface nitrogen abundances (e.g., Hunter et al., 2008). Those that are near-critical rotating are often correlated with having circumstellar disks, such as the Be stars, yet not in all cases such as the the fast rotating Bn stars.

3. Finally, *Polstar* will address processes that regulate the transfer of angular momentum. For example, around 10% of massive stars have surface magnetism at the kG level. Many of these have suffered significant magnetic braking. Separately, the Be stars may all have remnant companions from mass transfer (subdwarf O and B stars, white dwarfs, and even neutron stars or black holes) (Klement et al., 2019), and the Be stars are certainly fast (perhaps near-critical) rotators. The Be stars also have decretion disks, but these seems to come and go, with the star able to eject gas from its surface, and place it into orbits with higher specific angular momentum. *Polstar* will clarify how individual stars transport angular momentum throughout their interiors and in interactions with their immediate environments.

3.2. Polstar Observations

The *Polstar* design will make use of a Wollaston prism to split the light beam into ordinary and extraordinary rays to an echelle. Measurements will be obtained at 6 different modulator positions at selected orientation angles in order to optimize instrumental performance. The brightness throughput of the assembly depends on the polarization of the beam, and the 6 measurements can be used to invert (with optimization) to achieve full Stokes spectropolarimetry in I, Q, U, and V (refer to Scowen et al., 2022). We adopt the language that data taken at each modulator position is a subexposure; the 6 subexposures together are a single exposure; each visit to a target is an observation which may consist of multiple exposures plus all associated

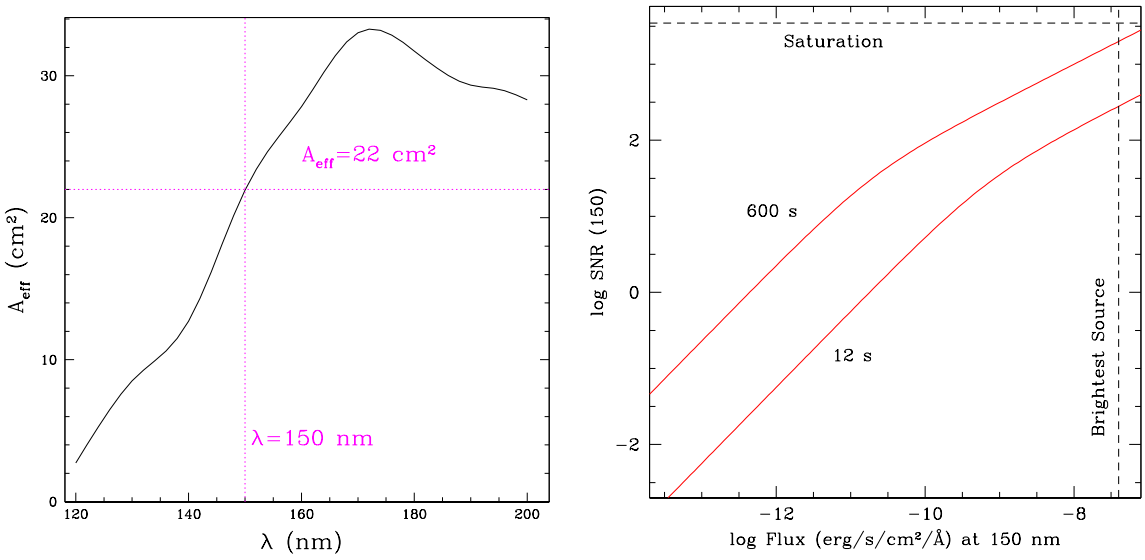

Figure 5: Left: Anticipated effective area of *Polstar*. Right: SNR values at 150 nm vs source flux. The two red curves are for an exposure of 12 and 600 s. The vertical dashed line is for our brightest source, Rigel. The horizontal dashed line is for saturation.

overtimes. As a concrete example, consider spectropolarimetry of a binary system with known period. Imagine data are collected at 20 equally spaced orbital phases, each visit having 2 exposures. This program would then consist of 20 observations, with 40 exposures, and 240 subexposures. There would be 240 total-light spectra and 40 polarized spectra produced. The subexposure time (for spectroscopy) or exposure time (for polarimetry) would be dictated by a signal-to-noise calculation in relation to the science requirements.

Using a model of Poisson statistics, we estimate the signal-to-noise ratio (SNR) for each spectral resolution element (hereafter "resel"). Each of the 6 orientation angles produces a spectrum, which are combined to obtain the polarization measures Q, U, and V. We estimate the SNR in terms of subexposures, from which SNR values for exposures, observations, and programs can be found. Refer to Table 2 for definitions of symbols appearing in the expressions that follow.

The signal is the source count rate multiplied by the subexposure time. The total noise, N_T, consists of source noise, dark current, and read noise, combined in quadrature as

$$N_T^2 = N_*^2 + N_D^2 + N_R^2 = \dot{S}_* \delta t + \dot{S}_D \delta t + N_R^2 \tag{3}$$

The resultant SNR in a subexposure becomes

$$SNR_{\rm sub} = \sqrt{\frac{\dot{S}_*^2 \, \delta t^2}{\dot{S}_* \, \delta t + \dot{S}_D \, \delta t + N_R^2}}. \tag{4}$$

As an example, the source count rate can be determined for known flux, using

$$\dot{S}_* = \frac{\lambda \, f_\lambda}{hc} \times A_{\rm eff}(\lambda) \times \frac{\lambda}{R}, \tag{5}$$

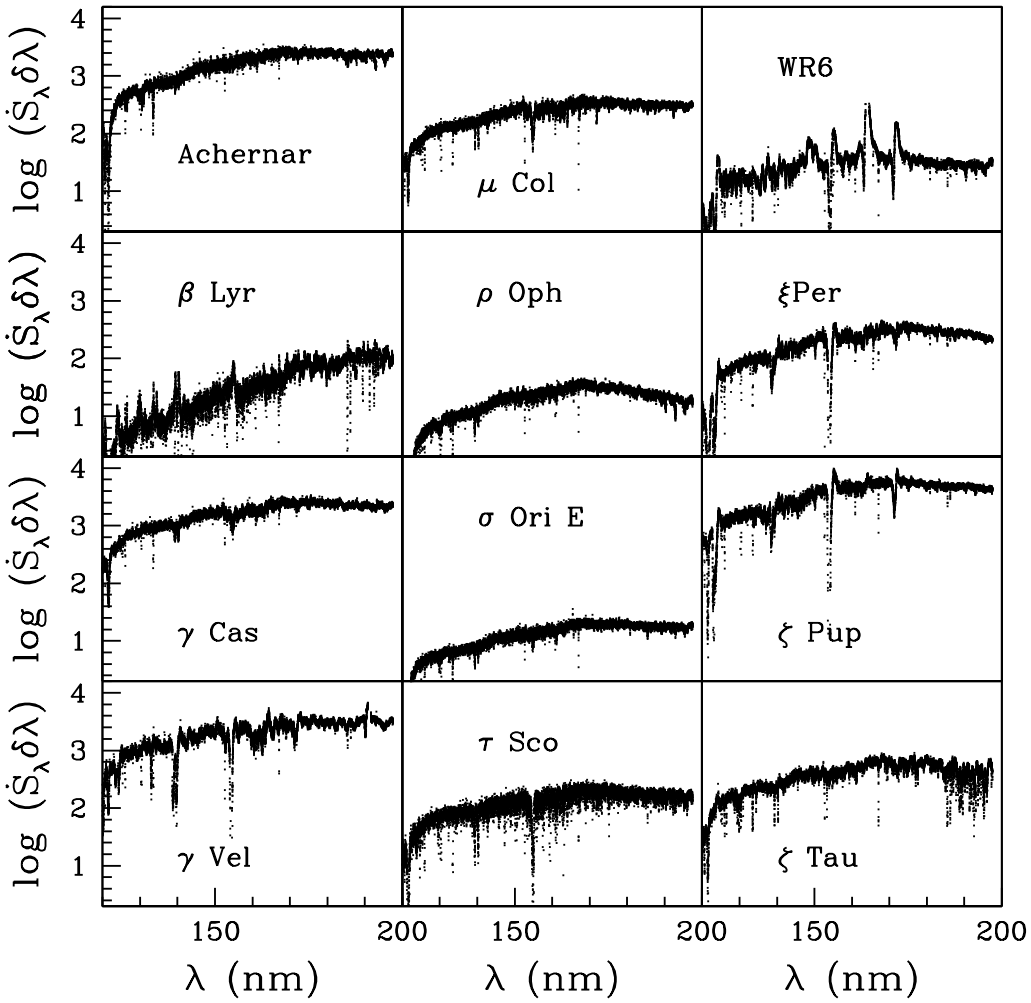

Figure 6: Simulated count rate spectra , involving the resel wavelength bin $\delta\lambda = \lambda/R$, for a selection of well-known massive stars using archival IUE spectra.

where f_λ is the source specific flux and $A_{\rm eff}(\lambda)$ is the effective area. Figure 5 shows the effective area with wavelength (left) and SNR performance as a function of f_λ at a reference wavelength of 150 nm (right). Additionally, Figure 6 provides example count rates per resel for some well-known massive stars using SWS IUE spectra.

Polstar will provide spectropolarimetric data of massive stars. Binning and stacking of exposures will provide high, medium, and low resolution spectroscopy with time to achieve diverse scientific requirements. For polarization many interesting effects arise at the level of 0.1%, requiring *SNR* values in excess of 1000 at the spectral resolution of interest. *Polstar* is baselined to provide polarimetric precision down to 0.03% in the most favorable cases.

4. Summary

Polarization is a powerful diagnostic for geometry in unresolved sources. The *Polstar* UV spectropolarimetry mission would provide sorely needed new capability to address several outstanding and fundamental questions that undergird massive star evolution, namely the exchange

of angular momentum between stars and its internal transport within them. A Guest Observer program is anticipated to provide important datasets in other areas of astrophysics (e.g., novae, chromospheres, exoplanets, and more).

Acknowledgments

RI gratefully acknowledges support from the National Science Foundation under grant number AST-2009412. Figures 1 and 3 are based on calculations kindly provided by J. P. Harrington and D. J. Hillier, respectively. The authors are indebted to the entire *Polstar* Team for their efforts past and present with developing and promoting the UV spectropolarimetry mission concept.

Further Information

ORCID identifiers of the authors

0000-0002-7204-5502 (Richard IGNACE)
0000-0002-9071-6744 (Paul SCOWEN)

Conflicts of interest

The authors declare that there are no conflicts of interest.

References

Bailey, J., Howarth, I. D., Cotton, D. V., Kedziora-Chudczer, L., De Horta, A., Martell, S. L., Eldridge, C. and Luckas, P. (2024a) Rapid polarization variations in the O4 supergiant ζ Puppis. MNRAS, 529(1), 374–392. https://doi.org/10.1093/mnras/stae548.

Bailey, J., Lewis, F., Howarth, I. D., Cotton, D. V., Marshall, J. P. and Kedziora-Chudczer, L. (2024b) Epsilon Sagittarii: An Extreme Rapid Rotator with a Decretion Disk. arXiv e-prints, arXiv:2407.11352. https://doi.org/10.48550/arXiv.2407.11352.

Belczynski, K., Bulik, T., Fryer, C. L., Ruiter, A., Valsecchi, F., Vink, J. S. and Hurley, J. R. (2010) On the Maximum Mass of Stellar Black Holes. ApJ, 714(2), 1217–1226. https://doi.org/10.1088/0004-637X/714/2/1217.

Clarke, D. (2010) Stellar Polarimetry.

Collins, I., George W., Truax, R. J. and Cranmer, S. R. (1991) Model Atmospheres for Rotating B Stars. ApJS, 77, 541. https://doi.org/10.1086/191616.

Domiciano de Souza, A., Kervella, P., Jankov, S., Abe, L., Vakili, F., di Folco, E. and Paresce, F. (2003) The spinning-top Be star Achernar from VLTI-VINCI. A&A, 407, L47–L50. https://doi.org/10.1051/0004-6361:20030786.

Donati, J. F. and Landstreet, J. D. (2009) Magnetic Fields of Nondegenerate Stars. ARA&A, 47(1), 333–370. https://doi.org/10.1146/annurev-astro-082708-101833.

Espinosa Lara, F. and Rieutord, M. (2011) Gravity darkening in rotating stars. A&A, 533, A43. https://doi.org/10.1051/0004-6361/201117252.

Folsom, C. P., Ignace, R., Erba, C., Casini, R., del Pino Alemán, T., Gayley, K., Hobbs, K., Manso Sainz, R., Neiner, C., Petit, V., Shultz, M. E. and Wade, G. A. (2022) Ultraviolet spectropolarimetry: investigating stellar magnetic field diagnostics. Ap&SS, 367(12), 125. https://doi.org/10.1007/s10509-022-04140-8.

Harmanec, P., Morand, F., Bonneau, D., Jiang, Y., Yang, S., Guinan, E. F., Hall, D. S., Mourard, D., Hadrava, P., Bozic, H., Sterken, C., Tallon-Bosc, I., Walker, G. A. H., McCook, G. P., Vakili, F., Stee, P. and Le Contel, J. M. (1996) Jet-like structures in β Lyrae. Results of optical interferometry, spectroscopy and photometry. A&A, 312, 879–896.

Harries, T. J., Hillier, D. J. and Howarth, I. D. (1998) A spectropolarimetric survey of northern hemisphere Wolf-Rayet stars. MNRAS, 296(4), 1072–1088. https://doi.org/10.1046/j.1365-8711.1998.01508.x.

Harrington, J. P. and Collins, I., George W. (1968) Intrinsic Polarization of Rapidly Rotating Early-Type Stars. ApJ, 151, 1051. https://doi.org/10.1086/149504.

Hillier, D. J. (1994) The calculation of continuum polarization due to the Rayleigh scattering phase matrix in multi-scattering axisymmetric envelopes. A&A, 289, 492–504.

Hoffman, J. L., Nordsieck, K. H. and Fox, G. K. (1998) Spectropolarimetric Evidence for a Bipolar Flow in beta Lyrae. AJ, 115(4), 1576–1591. https://doi.org/10.1086/300274.

Huang, W., Gies, D. R. and McSwain, M. V. (2010) A Stellar Rotation Census of B Stars: From ZAMS to TAMS. ApJ, 722(1), 605–619. https://doi.org/10.1088/0004-637X/722/1/605.

Hunter, I., Brott, I., Lennon, D. J., Langer, N., Dufton, P. L., Trundle, C., Smartt, S. J., de Koter, A., Evans, C. J. and Ryans, R. S. I. (2008) The VLT FLAMES Survey of Massive Stars: Rotation and Nitrogen Enrichment as the Key to Understanding Massive Star Evolution. ApJ, 676(1), L29. https://doi.org/10.1086/587436.

Ignace, R., Bjorkman, J. E., Chené, A. N., Erba, C., Fabiani, L., Moffat, A. F. J., Sincennes, R. and St-Louis, N. (2023) Modelling variable linear polarization produced by Co-rotating Interaction Regions (CIRs) across optical recombination lines of Wolf-Rayet stars. MNRAS, 526(1), 1298–1307. https://doi.org/10.1093/mnras/stad2878.

Ignace, R., Cassinelli, J. P. and Nordsieck, K. H. (1999) The Hanle Effect as a Diagnostic of Magnetic Fields in Stellar Envelopes. II. Some Theoretical Results for Resolved Line Profiles. ApJ, 520(1), 335–346. https://doi.org/10.1086/307435.

Ignace, R., Nordsieck, K. H. and Cassinelli, J. P. (1997) The Hanle Effect as a Diagnostic of Magnetic Fields in Stellar Envelopes. I. Theoretical Results for Integrated Line Profiles. ApJ, 486(1), 550–570. https://doi.org/10.1086/304512.

Klement, R., Carciofi, A. C., Rivinius, T., Ignace, R., Matthews, L. D., Torstensson, K., Gies, D., Vieira, R. G., Richardson, N. D., Domiciano de Souza, A., Bjorkman, J. E., Hallinan, G., Faes, D. M., Mota, B., Gullingsrud, A. D., de Breuck, C., Kervella, P., Curé, M. and Gunawan, D. (2019) Prevalence of SED Turndown among Classical Be Stars: Are All Be Stars Close Binaries? ApJ, 885(2), 147. https://doi.org/10.3847/1538-4357/ab48e7.

Kummer, F., Toonen, S. and de Koter, A. (2023) The main evolutionary pathways of massive hierarchical triple stars. A&A, 678, A60. https://doi.org/10.1051/0004-6361/202347179.

Langer, N. (2012) Presupernova Evolution of Massive Single and Binary Stars. ARA&A, 50, 107–164. https://doi.org/10.1146/annurev-astro-081811-125534.

Maeder, A. and Meynet, G. (2000) Stellar evolution with rotation. VI. The Eddington and Omega -limits, the rotational mass loss for OB and LBV stars. A&A, 361, 159–166. https://doi.org/10.48550/arXiv.astro-ph/0006405.

Nathaniel, K., Vigna-Gómez, A., Grichener, A., Farmer, R., Renzo, M. and Everson, R. W. (2024) Population synthesis of Thorne-Żytkow objects: Rejuvenated donors and unexplored progenitors in the common envelope formation channel. arXiv e-prints, arXiv:2407.11680. https://doi.org/10.48550/arXiv.2407.11680.

Nomoto, K., Kobayashi, C. and Tominaga, N. (2013) Nucleosynthesis in Stars and the Chemical Enrichment of Galaxies. ARA&A, 51(1), 457–509. https://doi.org/10.1146/annurev-astro-082812-140956.

Öhman, Y. (1946) On the Possibility of Tracing Polarization Effects in the Rotational Profiles of Early-Type Stars. ApJ, 104, 460. https://doi.org/10.1086/144879.

Penny, L. R. (1996) Projected Rotational Velocities of O-Type Stars. ApJ, 463, 737. https://doi.org/10.1086/177286.

Podsiadlowski, P., Joss, P. C. and Hsu, J. J. L. (1992) Presupernova Evolution in Massive Interacting Binaries. ApJ, 391, 246. https://doi.org/10.1086/171341.

Renzo, M., Zapartas, E., de Mink, S. E., Götberg, Y., Justham, S., Farmer, R. J., Izzard, R. G., Toonen, S. and Sana, H. (2019) Massive runaway and walkaway stars. A study of the kinematical imprints of the physical processes governing the evolution and explosion of their binary progenitors. A&A, 624, A66. https://doi.org/10.1051/0004-6361/201833297.

Sana, H., de Mink, S. E., de Koter, A., Langer, N., Evans, C. J., Gieles, M., Gosset, E., Izzard, R. G., Le Bouquin, J. B. and Schneider, F. R. N. (2012) Binary Interaction Dominates the Evolution of Massive Stars. Science, 337(6093), 444. https://doi.org/10.1126/science.1223344.

Scowen, P. A., Gayley, K., Ignace, R., Neiner, C., Vasudevan, G., Woodruff, R., Casini, R., Shultz, M., Andersson, B. G. and Wisniewski, J. (2022) The Polstar high resolution spectropolarimetry MIDEX mission. Ap. & Sp. Sci., 367(12), 121. https://doi.org/10.1007/s10509-022-04107-9.

Serkowski, K., Mathewson, D. S. and Ford, V. L. (1975) Wavelength dependence of interstellar polarization and ratio of total to selective extinction. ApJ, 196, 261–290. https://doi.org/10.1086/153410.

St-Louis, N., Tremblay, P. and Ignace, R. (2018) Polarization light curve modelling of corotating interaction regions in the wind of the Wolf-Rayet star WR 6. MNRAS, 474(2), 1886–1899. https://doi.org/10.1093/mnras/stx2813.

Stenflo, J. (1994) Solar Magnetic Fields: Polarized Radiation Diagnostics, vol. 189. https://doi.org/10.1007/978-94-015-8246-9.

Stenflo, J. O. (2013) Solar magnetic fields as revealed by Stokes polarimetry. A&ARv, 21, 66. https://doi.org/10.1007/s00159-013-0066-3.

Toonen, S., Portegies Zwart, S., Hamers, A. S. and Bandopadhyay, D. (2020) The evolution of stellar triples. The most common evolutionary pathways. A&A, 640, A16. https://doi.org/10.1051/0004-6361/201936835.

Ud-Doula, A., Owocki, S. P. and Townsend, R. H. D. (2009) Dynamical simulations of magnetically channelled line-driven stellar winds - III. Angular momentum loss and rotational spin-down. MNRAS, 392(3), 1022–1033. https://doi.org/10.1111/j.1365-2966.2008.14134.x.

Vink, J. S. (2022) Theory and Diagnostics of Hot Star Mass Loss. ARA&A, 60, 203–246. https://doi.org/10.1146/annurev-astro-052920-094949.

von Zeipel, H. (1924) The radiative equilibrium of a rotating system of gaseous masses. MNRAS, 84, 665–683. https://doi.org/10.1093/mnras/84.9.665.

Whittet, D. C. B., Martin, P. G., Hough, J. H., Rouse, M. F., Bailey, J. A. and Axon, D. J. (1992) Systematic Variations in the Wavelength Dependence of Interstellar Linear Polarization. ApJ, 386, 562. https://doi.org/10.1086/171039.